



A High-Resolution Framework for Urban Pluvial Flood Risk Mapping

Anastasia Vogelbacher^{1,2*}, Malte von Szombathely^{*3}, Marc Lennartz⁴, Benjamin Poschlod³ and Jana Sillmann³

5 ¹ Institute of Geo-Hydroinformatics, Hamburg University of Technology, Institute of Geo-Hydroinformatics, Hamburg, Germany

²United Nations University Hub on Engineering to Face Climate Change at the Hamburg University of Technology, United Nations University Institute for Water, Environment and Health (UNU-INWEH), Hamburg, Germany

10 ³Research Unit Sustainability and Climate Risk, Center for Earth System Research and Sustainability (CEN), Universität Hamburg, Grindelberg 5, 20144 Hamburg, Germany

⁴Section Hydrology, GFZ Helmholtz Centre for Geosciences, P.O. Box 60 12 03, 14412 Potsdam, Germany

Correspondence to: Malte von Szombathely (malte.szombathely@uni-hamburg.de), Anastasia Vogelbacher (anastasia.vogelbacher@tuhh.de)

15

Abstract. This study presents a high-resolution framework for assessing climate-related risk at the building scale by operationalizing the IPCC risk concept, defining risk as a function of vulnerability, exposure and hazard. The framework focuses on pluvial flood risk related to people's well-being and mobility. Hazard is driven by a 100-year rainfall event (36 mm h⁻¹), modelled with a hydrodynamic flood simulation incorporating topography, drainage capacity, and land use.

20 Exposure is differentiated by impact type, considering residents on ground floors for well-being and building proximity to flooded streets for mobility and accessibility. Social vulnerability is quantified using socioeconomic indicators such as age, income, and education. The framework is demonstrated using empirical data from Hamburg, Germany, identifying risk hotspots where high social vulnerability coincides with elevated flood exposure. To support practical implementation, we introduce a Python-based ArcGIS pluvial flood risk toolbox that enables automated, building-level risk mapping. The 25 transparent and flexible design makes the framework transferable to other cities, supporting climate adaptation planning and risk-informed decision-making.

Non-Technical Summary

With more than half of the population living currently in urban settings and increased urbanization under changing climate leads to the need of assessing risk to climate extremes, such as pluvial flooding at local scale. In this study, this is addressed 30 by following the Intergovernmental Panel on Climate Change (IPCC) risk definition, conceptualizing risk as a function of hazard, exposure, and vulnerability. The resulting risk is presented as risk to well-being, considering residents living on the building's ground floor and the risk to mobility and accessibility, taking into account flooded streets in close vicinity to the building. The results identify buildings in urban areas where residents face higher flood risk due to greater social



vulnerability, increased exposure, or elevated flood hazard. We present the development and application of a Python-based
35 ArcGIS toolbox for estimating pluvial flood risk at the building scale. It is designed specifically for application in urban environments. This allows city planners to target the areas most in need of attention. The approach is transferable to other cities, offering a practical tool for flood risk management and climate adaptation planning.

1 Introduction

More than half of the world's population (55%) currently resides in urban areas, a figure projected to increase to 68% by
40 2050 (United Nations, 2019). Urbanization, coupled with climate change, intensifies the risk of pluvial flooding, especially in strongly sealed cities where intense rainfall leads to small-scale, rapid flooding events (Arnbjerg-Nielsen et al., 2013; Fereshtehpour & Najafi, 2025; Scalenghe & Marsan, 2009). Climate change already exacerbates short-duration rainfall extremes (Lang & Poschlod, 2024), with further intensification expected under warming scenarios (Fowler et al., 2021). Recent studies emphasize the importance of understanding these extreme events at high temporal and spatial resolutions, as
45 they significantly influence urban flood risk assessments (Sillmann et al., 2024).

While many modelling approaches for pluvial flood hazard and vulnerability assessment exist, their effectiveness depends heavily on data availability and local conditions (Bulti & Abebe, 2020; Cea & Costabile, 2022; Nkwunonwo et al., 2020). High-resolution models are essential for credible risk assessments and effective flood management strategies (Fritsch et al., 2016; Rehman et al., 2019). In this context, the development of practical, stakeholder-oriented tools that incorporate a
50 holistic perspective is crucial for urban resilience efforts.

Previous work on high-resolution flood risk management mainly focused on the hazard component, e.g. by integrating high-resolution flood modelling (Bertsch et al., 2022). However, only a few cases expanded the hazard-focused few by incorporating additional variables into the risk estimation, such as susceptibility and exposure at the basin scale (Afifi et al., 2019; Devi et al., 2025) or the building usage to estimate the damage potential (Bhola et al., 2020). Other studies linked
55 citizen science to flood modelling (Assumpção et al., 2018). Notably, certain projects have used physically-based damage modelling approaches to quantify risk more precisely (e.g. Gentile et al., (2022), providing valuable insights for urban flood risk management. However, the integration of all three variables, hazard, exposure and (social) vulnerability remains largely unaddressed on this scale.

The current work builds on these foundations by focusing on user-friendly, stakeholder-oriented tools and goes beyond
60 existing approaches. The proposed framework implements the Intergovernmental Panel on Climate Change (IPCC) risk definition, conceptualizing risk as a function of hazard, exposure, and vulnerability (Field et al., 2014). To tailor this framework for an urban context, we adapt the social vulnerability concept articulated by von Szombathely et al. (2023), specifically focusing on its application to pluvial flood hazards on a building-resolving scale. This approach emphasizes the importance of understanding social dynamics in risk assessments, aligning with recent research efforts that aim to integrate
65 hazard-specific vulnerability profiles within urban settings (Alves et al., 2021; Prall et al., 2024).



This methodological paper aims to develop and demonstrate a comprehensive risk mapping framework for pluvial flooding. The framework has already been applied to an analysis of pluvial flood risk in Hamburg, Germany (von Szombathely et al., in review). Central to this effort is the creation of a stakeholder-informed Python-based ArcGIS toolbox designed to generate flood risk maps, supporting urban stakeholders in flood risk management. By exemplifying an approach applicable to other 70 cities, this framework seeks to promote reproducibility and transferability in urban flood risk assessments, where stakeholder and flood risk managers can holistically assess flood risk providing information at building-resolving scale. We follow the FAIR Principles (Findable, Accessible, Interoperable, Reusable), ensuring that both data and methods are transparently shared and can be used effectively by other cities (Wilkinson et al., 2016). With this approach, we aim to bridge the gap 75 between technical flood hazard modelling and decision-oriented risk management, enabling more informed, transparent, and inclusive urban flood risk planning.

2 Data and Software Environment

For this analysis, we use the ArcGIS Pro Software and the Python programming language to ensure both professional functionality and open-source adaptability. ArcGIS Pro is a license-based software and for this analysis, the advanced license is used. Since ESRI products are widely used among the involved stakeholders, the primary application presented here is 80 based on the ArcGIS Pro environment. More specifically, we employ the Model Builder tool, which enables users to sequence geoprocessing tools and package them into reproducible workflows, also known as toolsets, which are organized within a toolbox. This approach allows others to easily replicate the analytical steps described in this study.

To ensure transparency and facilitate open-source data replication, all models created using the Model Builder were also exported as Python scripts, allowing users to run or modify them outside the ArcGIS environment.

85 2.1 Input data

For the implementation of the toolbox, we create synthetical data derived from publicly available datasets provided by the City of Hamburg, Germany, as described in von Szombathely et al., (in review). The following Table 1 summarizes the data used in this analysis. However, even though based on real empirical data from Hamburg, we aim to anonymize building-level data to prevent identification of individual households and show the applicability to other urban environments on 90 building-scale. We describe the data preparation in the following. An excerpt of the input data layer is visible in Figure S1.



Table 1: Input data overview.

Raw variable		Derived variables	Resolution	Output variables	Source
Social Vulnerability	Socio-economic data	Number of children < 10 years old (C)	Statistical unit	SV _{PF}	FHH, Behörde für Stadtentwicklung und Wohnen, (2023) FHH, Statistikamt Nord, (2024)
		Elderly singles > 65 years old (ES)			
		People without high school diploma within the last 3 years (EDQ)			
		Receivers of social welfare (WR)			
Exposure	Residents data	Residents per building (R) and residents per ground floor level (RG)	Statistical unit	E _{MA} , E _{WB}	FHH, Statistikamt Nord, (2024)
	Infrastructure	Street outlines	m	Intersected areas with flood layer	FHH, Statistikamt Nord, (2017)
	Building information	Nr. of floors above ground and building type	Building level	E _{MA} , E _{WB}	Landesbetrieb Geoinformation und Vermessung (LGV) Hamburg, (2020)
Hazard	Flood data	Water level based on pluvial flood scenario based on a rainfall of 36 mm/h reflecting a 100-year event	m ²	H _{MA} , H _{WB}	FHH, BUKEA, (2024)

2.2 Social Vulnerability: Socio-economic data

The underlying demographic and socio-economic data are based on the data provided for the city of Hamburg and available at the resolution of statistical units, where statistical units are sub-regions reflecting a grouping of neighbouring building blocks that are assumed to be homogeneous in terms of their building and socio-structural characteristics (Statistisches Amt für Hamburg und Schleswig-Holstein, 2024). For our analysis numbers of children under 10 years old and singles over 65 years old are required to reflect the sensitivity to flood hazards. To demonstrate coping capacity, data on social welfare recipients and the number of residents who left school without a high school diploma within the last three years is used (FHH, Behörde für Stadtentwicklung und Wohnen, 2023, 2024; Statistisches Amt für Hamburg und Schleswig-Holstein, 2024). This information is the only available data source providing information on the high school level for the case study



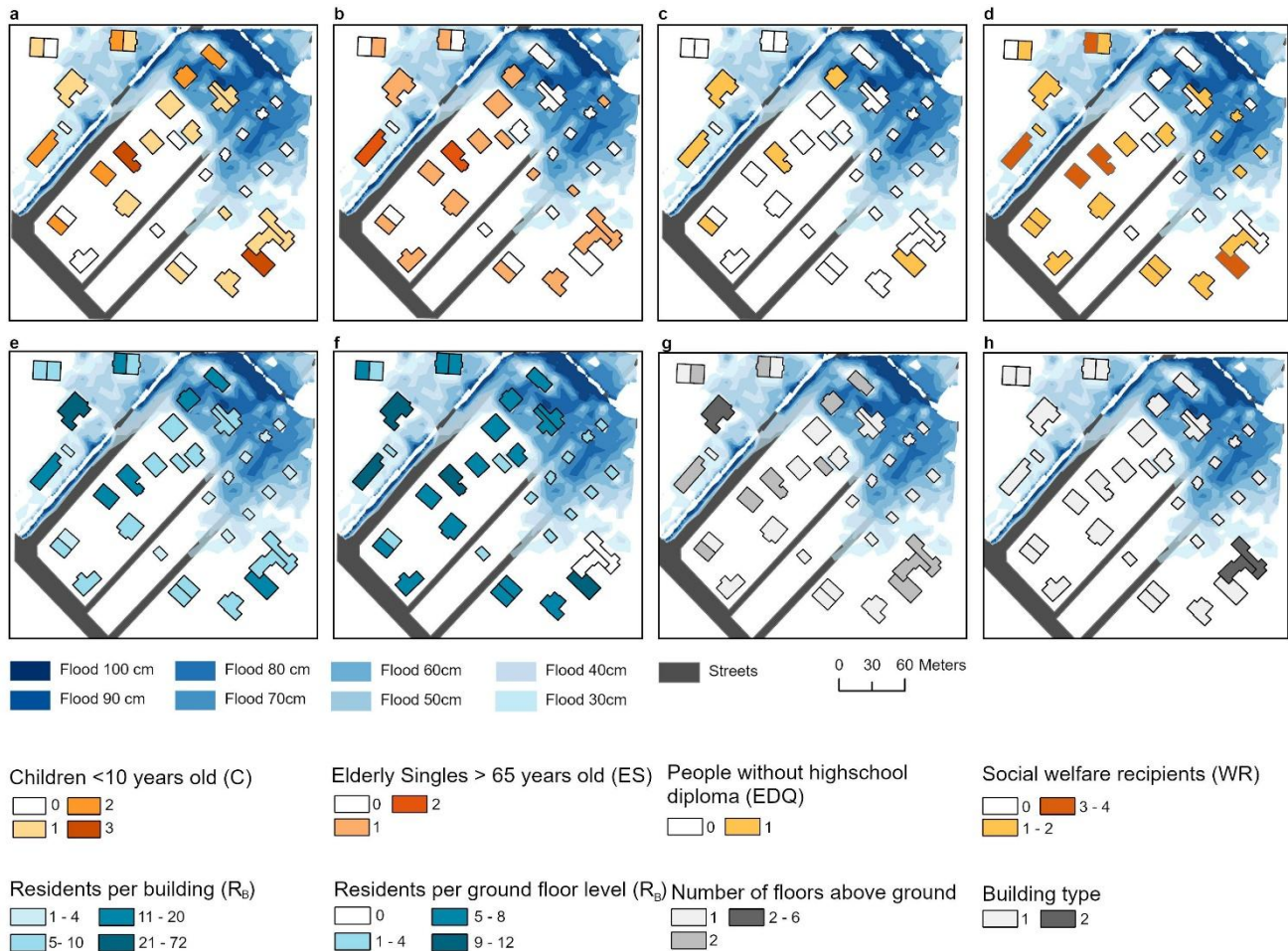
105 example. As this data is only publicly available aggregated for the whole statistical unit due to data protection, we
disaggregated the data using the toolbox to the building level creating one possible realization guided by expert knowledge,
reproducing the total numbers of the statistical unit. This allows us to show the capabilities of the toolbox at building-
resolving scales. As socio-economic data is often available at aggregated scales, the toolbox also offers the functionality to
disaggregate the data linearly across a statistical unit as shown in von Szombathely et al., (2023). However, for the case
110 study, a linear disaggregation would result in a completely homogeneous spatial distribution of socio-economic data, which
is not well suited to show the implications of high-resolution risk mapping at the building-resolving scale.

2.3 Exposure: Residents and infrastructure data

Due to data protection regulations, information on the number of residents in each building is not publicly available for
German cities, like Hamburg. Instead, 2023 population data is reported at the statistical unit level (Statistisches Amt für
115 Hamburg und Schleswig-Holstein, 2024). Hence, we distribute the number of residents to the buildings of the case study
guided by the living space of the buildings. For the spatial analysis, we use road data from 2019 and building outlines from
2020, including the number of above-ground floors and their primary function (residential or mixed-use). Both datasets are
sourced from the official land register (ALKIS) provided by the city of Hamburg (FHH, Statistikamt Nord, 2017;
Landesbetrieb Geoinformation und Vermessung (LGV) Hamburg, 2020).

120 **2.4 Hazard: Modelled flood level data**

Simulations of pluvial flooding are provided by Hamburg's water supply and wastewater disposal company HAMBURG
WASSER on behalf of and in cooperation with the Hamburg Ministry for Environment, Climate, Energy and Agriculture
(Behörde für Umwelt, Klima, Energie und Agrarwirtschaft; BUKEA). Our case study example is based on the pluvial flood
125 scenario triggered by a design rainfall of 36 mm/h reflecting a 100-year event (FHH, BUKEA, 2024), assuming a uniform
probability of occurrence throughout the urban area with a resolution of 1 m². In sum, the input data of our case study is
based on empirical data of one statistical unit from Hamburg reproducing the total numbers of the official city statistics,
while the disaggregation to the building level does not reflect real observed conditions. Though, we argue that the resulting
case study data are a plausible realization of socio-economic data, exposure and hazard reflecting the spatial variability
within a city quarter. The input data of the here shown case study are publicly available
130 (<https://doi.org/10.5281/zenodo.17986182>).



135 **Figure 1: Underlying input data for the risk map framework.** The first row (a to d) includes social vulnerability parameters, whereas
 the bottom row (e to h) shows exposure related variables. Hazard related variables are depicted as flooding depths between 30 and 100 cm.

3. Methodology

The applied input data and overall structure of the here presented methodology is presented in Fig. 2. The figure illustrates the methodological framework developed to assess pluvial flood risk (PFR) by integrating Social Vulnerability (SV), Exposure (E), and Hazard (H). Each component is processed separately based on its native data structure and subsequently
 140 harmonized to a common spatial resolution (building polygons) before the final risk calculation.

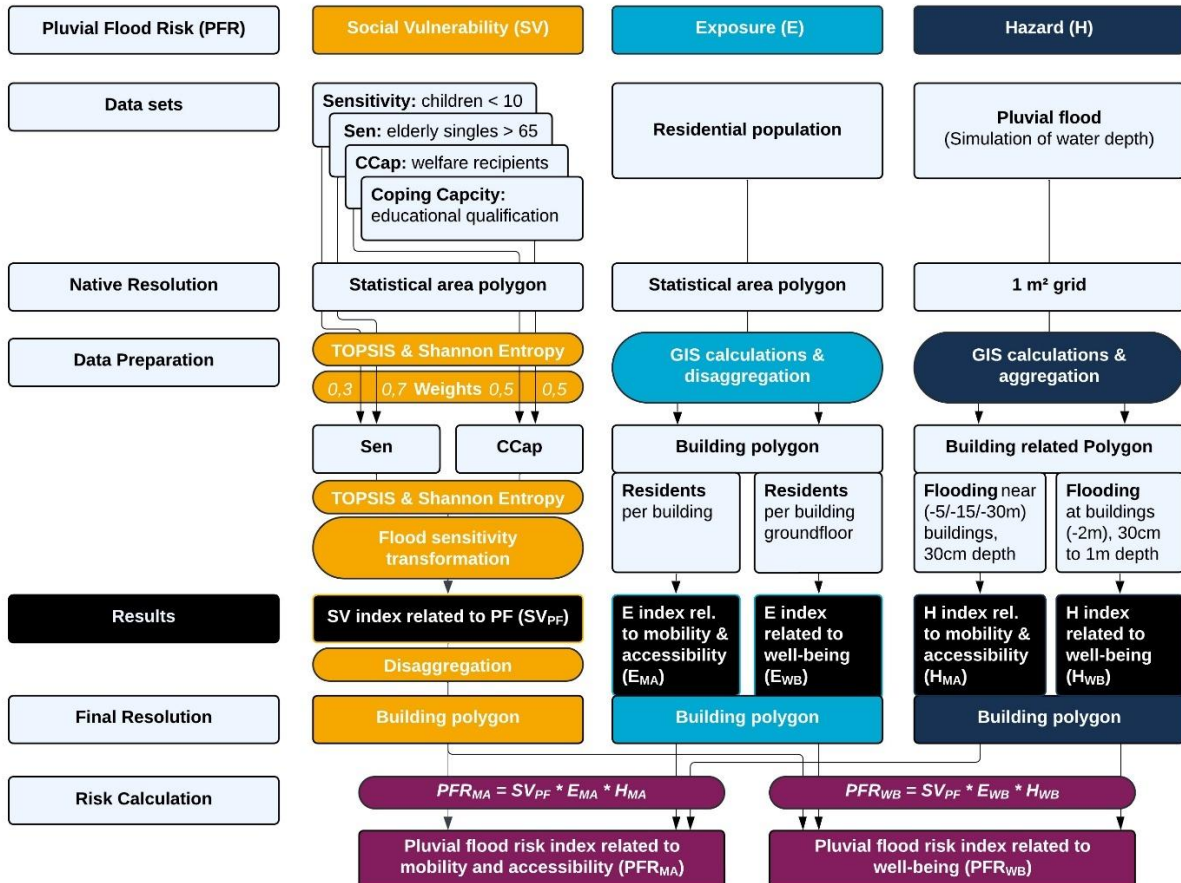


Figure 2: Overview of the applied methodology for calculating pluvial flood risk at the household level in an exemplary urban environment. Colours and labels indicate the individual components and processing steps of the risk calculation.

145 The structure of the framework also serves as the structure for this chapter. Section 3.1 describes the conceptual design and data preparation for each column. Section 3.2 then shows the exact calculation and implementation in the ArcGIS toolbox.

3.1 Underlying concepts and data pre-processing

3.1.1 Social Vulnerability

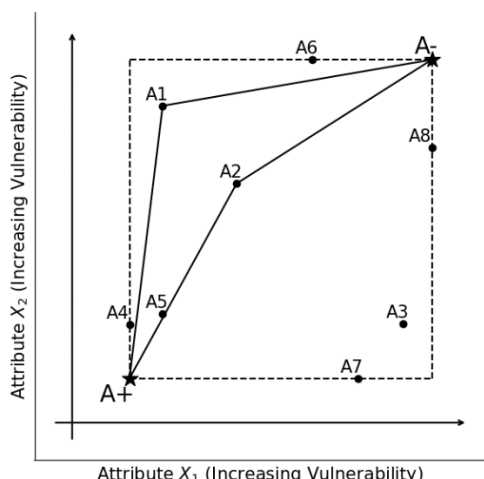
150 The concept of SV is based on the selection of socio-economic variables that must be related to each other. Each increase of each variable must increase vulnerability and the assigned variables should be categorized in either Sensitivity or Coping Capacity for flood events. It is important to ensure that horizontal social distinctions (such as age) contribute to sensitivity, while vertical distinctions (such as income) (Bourdieu, 1984) influence coping capacity.



For the calculation of social vulnerability (SV) we followed the procedure presented in von Szombathely et al., (2023),
155 where SV is calculated considering the coping capacity and sensitivity, both represented with equal importance (0.5, 0.5).
These weights are based on an analytical hierarchy process and local expert opinions. All weights in either the group of
sensitivity or coping capacity have to add up to one. In the case study, sensitivity is defined by assigning a weight of 0.7 to
children under 10 years old (C) and 0.3 to elderly singles over 65 years old (ES). For coping capacity, equal importance (0.5)
160 are used between the number of residents who left school without a high school diploma within the previous three years
(EDQ) as well as recipients of social welfare (WR).

Since we include several variables that contribute to a combined flood risk index, it is important to consider how these
variables interact to create a comprehensive assessment of flood risk. While the alternatives can be easily ranked based on a
single attribute, combining all attributes into a single index requires special techniques. One method in flood risk analysis is
165 the Technique for Order Performance by Similarity to an Ideal Solution (TOPSIS) (Hwang & Yoon, 1981) which has been
applied in several flood risk analysis' (Ekmekcioğlu et al., 2021; Nguyen et al., 2020; Pathan et al., 2022; Rafiei-Sardooi et
al., 2021; Yang et al., 2018) and was applied in this work in addition to the methodology presented in von Szombathely et al.
von Szombathely et al., (2023). This technique quantifies for each alternative (A1 - A8 in Figure 3) the relative distance to
the positive ideal (A+ in Figure 3) and negative ideal (A- in Figure 3) and ranks them accordingly.

The TOPSIS method can compare attributes with differing units and is able to incorporate specific weights for each attribute.
170 The values assigned to each alternative can also be interpreted geometrically: for each attribute, the maximum (A⁻) and
minimum (A⁺) values define two ideal points within a multidimensional space. The dimension is equal to the number of
different attributes. Then each alternative occupies a place in space. Lastly, we can calculate the relative Euclidean distance
to the negative and positive ideal (A⁻, A⁺ see Figure 3).



175 **Figure 3: Conceptual description of social vulnerability (adapted from Dyson et al., (2017)).** A- and A+ represent negative and
positive ideals of the vector space (dashed lines) spanned by the smallest and largest attributes of the alternatives (A1 to A8). The solid
lines depict the distance between two example points (A1 and A2) to either ideal point.



Heterogeneity may be a driving factor in the way attributes contribute to the final risk index. This is not considered in the TOPSIS approach but can be compensated by applying the Shannon Entropy method (Shannon, 1948). Other studies have
180 already applied this concept in a flood risk context (Malekinezhad et al., 2021; Yang et al., 2018). In our analysis, both the TOPSIS and the Shannon Entropy methods are applied to the estimation of Sensitivity, Coping Capacity and the Social Vulnerability Index (SVI).

The distribution of the Social Vulnerability Index depends heavily on the variability of the initial socio-economic data, which is in turn dependent on the spatial resolution of the socio-economic data. Since we aim for an application of the IPCC
185 risk framework to urban pluvial flood risk, it would be ideal to have socio-economic data at the building resolution. The coarser the resolution of the input variables used to calculate the SVI, the more the SVI follows a normal distribution. Given that our analysis is applying the risk framework at the household level, the social vulnerability data is skewed. When multiplying the social vulnerability with the exposure and hazard indices as foreseen by the IPCC risk framework, the skewed social vulnerability data would affect the final risk index less compared to exposure and hazard. To mitigate this, we
190 square social vulnerability values to approximate a more normal distribution of SVI values.

In addition, we address the implication of the IPCC risk framework, which defines risk as the product of hazard, exposure, and social vulnerability, and would therefore assign zero risk to observations with “no” social vulnerability. In the case of the proposed SVI depending on age, social welfare and the high school diploma, zero values of the SVI are possible on the building scale. To prevent that this leads to zero risk, a value of a quarter mean of the SV value is added to the SV value.
195 This is an arbitrary choice and we acknowledge the possible variations of resulting risk. Therefore, we show the effect of varying transformation thresholds on the overall estimated risk within the sensitivity analysis (Section 4.1).

3.1.2 Exposure

In line with the IPCC framework, we define exposure as the presence of people in areas that may be adversely affected by pluvial flooding. In this study, exposure is assessed in relation to the residential population and their places of residence.
200 Since different flood hazards have varying impacts, we differentiate between hazards to mobility restrictions & accessibility and hazards to well-being, leading to two distinct exposure concepts:

1. **Exposure related to mobility & accessibility (E_{MA})**: Includes all residents of a given building, as flooding can affect their ability to enter or exit the premises.
2. **Exposure related to well-being (E_{WB})**: Considers only individuals residing on the ground floor, as they are directly affected by water entering the building.

In case of aggregated input data, the toolbox can allocate population data at the building level, assuming a uniform population distribution within each statistical unit. The total population is then distributed among residential buildings in proportion to their available living space. In the case of mixed-use buildings, we assume that the first floor is dedicated to commercial use and does not contribute to the residential living area. This method improves the spatial accuracy of our
210 exposure assessment by ensuring a more realistic distribution of inhabitants.



3.1.3 Hazard

In this study, we only consider urban pluvial flooding as the hazard. We define water level thresholds based on existing studies on pluvial flooding (Bhola et al., 2020; Calianno et al., 2013; Lazzarin et al., 2022) and building regulations (Bignami, 2019). Following the two distinct exposure concepts we define two pluvial flood hazards:

215 1. **Hazard related to well-being (H_{WB})**: Water levels from 30 cm to 1 m with 10 cm increments directly adjacent to buildings, to assess the potential for damage and danger to well-being.

2. **Hazard related to mobility and accessibility (H_{MA})**: 30 cm as a threshold for flooding near buildings, to evaluate how flooding impacts movement and access in affected areas.

3.1.4 Risk

220 Building on the previously established data indices, flood risk at the building level is assessed using the IPCC Risk Assessment framework (Intergovernmental Panel On Climate Change (Ipcc), 2021), which integrates hazard, exposure, and vulnerability to quantify risks associated with pluvial flooding. This approach enables a detailed evaluation of flood-related impacts on mobility & accessibility and well-being in Hamburg. Based on this conceptual decision to define two different approaches to hazard and exposure, we ultimately calculate two different risk indices:

225 1. **Pluvial flood risk to well-being (PFR_{WB})**
2. **Pluvial flood risk to mobility and accessibility (PFR_{MA})**

3.2 Toolbox Architecture and Model Development

230 To adopt the theoretical concepts into reproducible workflows, we made use of the ArcGIS Pro (V.3.2.0) model builder. We created a Risk Map Toolbox (<https://doi.org/10.5281/zenodo.17986182>), which contains all calculation steps needed to represent the here shown results. The tools are stored in three toolsets, following the presented structure of the IPCC including Vulnerability, Exposure and Hazard (Figure 4). For the final risk calculation, a script-based tool is added, as well as an optional tool which calculates the boundary classes used for the applied visualization.

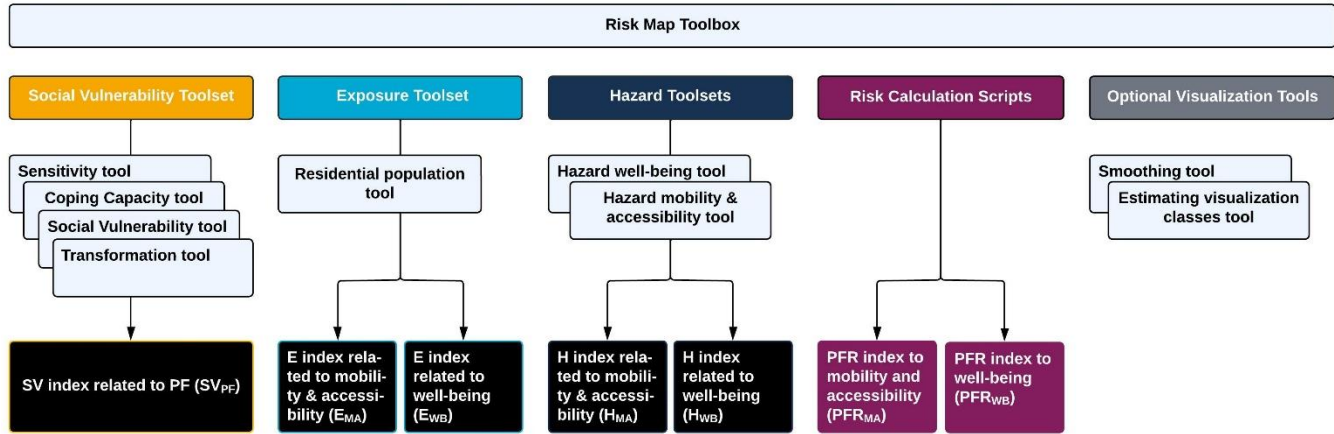


Figure 4: Outline of the Risk Map Toolbox. The coloured boxes represent the corresponding risk parameters (Social Vulnerability, 235 Exposure, Hazard, and Risk Calculation), containing toolsets and scripts for the respective calculation steps. Black boxes represent the result(s) of each Toolset, necessary for risk calculation (dark purple boxes). For an overview of the appearance in ArcGIS and the actual user interfaces, please refer to Figure S14.

3.2.1 Social Vulnerability Toolset

The SV toolset calculates Sensitivity, Coping Capacity, and the SV index using TOPSIS, and its transformed version using 240 the flood sensitivity transformation tool. Each vulnerability tool allows adjustment of the weights for Sensitivity and Coping Capacity. Within each group, the weights must sum to one and can be modified in the toolbox (Equ. 1 - 3).

$$SV_i = F_{TOPSIS}(CC_i, S_i, 0.5, 0.5) \quad , \text{with} \quad (1)$$

$$CC_i = F_{TOPSIS}(C_i, ES_i, 0.3, 0.7) \quad , \text{and} \quad (2)$$

$$S_i = F_{TOPSIS}(WR_i, EDQ_i, 0.5, 0.5) \quad (3)$$

245

where the TOPSIS procedure is represented as F_{TOPSIS} for the coping capacity (CC_i), and Sensitivity (S_i), for each alternative (building) i .

In more detail, to apply TOPSIS, all attributes are normalized (Eq. 4), and then multiplied with the specific weight. The normalization of each alternative can be expressed as:

$$250 \quad z_{ij} = \frac{x_{ij}}{\sum_{i=1}^m x_{ij}}, j \in \{1, \dots, n\}, i \in \{1, \dots, m\} \quad (4)$$

where z_{ij} is the normalized attribute and x_{ij} reflects the unweighted value for the i -th alternative (buildings) and j -th attribute (relative share of C, ES, WR, EDQ).

The maximum and minimum values for each attribute define two ideal points in a multidimensional space (Eq. 5). We can 255 calculate the relative Euclidean distance to this negative and positive ideal (A-, A+ see Figure 3). Generally speaking for alternative A_i with n different attributes, let z_{ij} be the normalized attribute then:



$$F_{TOPSIS}(z_{i1}, \dots, z_{in}, w_1, \dots, w_n) = \frac{\sqrt{\sum_{j=1}^n w_j^2 (min_i(z_{ij}) - z_j)^2}}{\sqrt{\sum_{j=1}^n w_j^2 (min_i(z_{ij}) - z_j)^2} + \sqrt{\sum_{j=1}^n w_j^2 (max_i(z_{ij}) - z_j)^2}} \quad (5)$$

with n attributes, where z_{ij} is the normalized attribute and j_{th} reflects the unweighted attribute for the i_{th} alternative.

Additionally, we apply the Shannon Entropy method. The idea of the Shannon Entropy method is to multiply the final risk index with an entropy-index between 1 and 2, where 1 indicates complete homogeneity and 2 indicates total inhomogeneity across different attributes. More specifically, for m alternatives with n attributes, where z_{ij} is the normalized attribute and j_{th} reflects the unweighted attribute for the i_{th} alternative, the entropy U_i is calculated following Eq. 6:

$$U_i = 2 + \frac{1}{\ln(n)} \sum_{j=1}^n \left(\frac{z_{ij}}{\sum_{j=1}^n z_{ij}} \ln \left(\frac{z_{ij}}{\sum_{j=1}^n z_{ij}} \right) \right), i \in \{1, \dots, m\} \quad (6)$$

The effect of heterogeneity depends on the specific context and its application should be evaluated individually for each hazard scenario. Hence, our toolbox offers the user to choose if Shannon Entropy shall be applied (please see additional screenshots of the tool user interfaces provided in the supplementary material Figure S2 a to c.).

Finally, we perform two additional transformations, addressing the specific data distribution of SV (flood sensitivity transformation, see Fig. 1): (a) To mitigate the skewed social vulnerability data, we square social vulnerability values to approximate a more normal distribution of SV values; (b) to prevent that zero SV values lead to zero risk, a value of a quarter mean of the SV value is added to the SV value (see Eq. 7). This threshold must be evaluated individually for different hazards or cities. Hence, our toolbox offers the user to apply different thresholds if needed (no, half or one mean value)

$$SV_{PF} = \left(U_i \cdot SV + \frac{Mean(U_i \cdot SV)}{4} \right) \quad (7)$$

, with the Entropy U_i , and the previously calculated social vulnerability value (SV).

All four tools are coded in Python and were incorporated within the ArcGIS framework. An exemplary outline of the calculated values is depicted in Figure S3. We show the sensitivity to changes of this threshold within the sensitivity analysis.

3.2.2 Exposure Toolsets

The calculation of Exposure contains one tool (see Figure 4) including several sub-tools which are linked to one-another. The full workflow exported from the toolbox can be viewed in the supplementary Figure S4. First, both input data, the available data based on the statistical unit and the building information are combined (See Figure S5 a to c). Then, the available living area per building is calculated based on the following equation (Fig. S5 d and e) (Eq. 8).

$$A_B = (Fl - (B - 1)) \cdot A_P \quad (8)$$



285 Where A_B is the area of each building (in m^2), Fl being the number of floors of the corresponding building and B the building type, ($B = 1$ for residential, $B = 2$ for mixed use, containing no residents on the base floor level but in the upper levels), and A_P for the area (in m^2) of each building.

Following the two previously mentioned exposure concepts of E_{MA} , including all residents of a given building and E_{WB} , considering only individuals residing on the ground floor level, the subsequent Eq. 9 and Eq. 10 are used to obtain E_{MA} and

290 E_{WB} .

$$E_{MA} = \frac{A_B}{A_{LSU} \cdot R_{SU}} \quad (9)$$

with A_B being the area in m^2 of each house, A_{LSU} the total living area in m^2 within the statistical unit and R_{SU} , the overall number of residents living in the corresponding statistical unit (SU).

$$E_{WB} = \frac{(-(B-2) \cdot E_{MA})}{Fl} \quad (10)$$

295 With building type ($B = 1$ for residential, $B = 2$ for mixed use) and the number of floors in the corresponding house (Fl).

The corresponding tools are shown in Fig. S5 e to i). An excerpt of the resulting attribute table after implementing the exposure calculation is depicted in Figure S6.

3.2.3 Hazard Toolsets

The calculation of the hazard is two-fold, one toolset is developed for the calculation of the hazard to mobility & 300 accessibility and one for the hazard to well-being.

The assessment of the hazard to well-being is carried out in two stages (see Fig. S7). The first tool computes the areas of intersection between all flood-depth layers from 30 cm to 100 cm (with 10 cm increments) and the affected buildings (see Fig. S7 a and c). To account for potential water intrusion near buildings, we applied a 2-meter buffer around all buildings, which was determined based on the native 1-meter resolution of the flood simulation, expert knowledge, and stakeholder 305 workshops in Hamburg, as well as following the approach of von Szombathely et al., (in review).

The second tool (as shown in Fig. S7 b) calculates the hazard to well-being (H_{WB}) following a cumulative distribution function (CDF; Φ) of the log-normal distribution with $\mu = 0$ and $\sigma = 0.25$.

$$F_X(x) = \Phi\left(\frac{\ln(\ln(x)) - \mu}{\sigma}\right) \quad (11)$$

We derive the hazard index with

$$310 \quad H_{WB} = \sum_{i=30}^{100} [F_X(4 \cdot A_{2m,i})], \quad i \in \{30, 40, 50, 60, 70, 80, 90, 100\} \quad (12)$$

where $A_{2m,i}$ as the fraction of the flooded area within a 2 m buffer at the water level i (in centimeter).

The toolset of the well-being hazard considers all potential flood-layers included in the corresponding input folder. In the sensitivity analysis, we therefore discuss the sensitivity of the applied method using a lower flooding threshold (20 cm). An example of the resulting output table is shown in Figure S8.



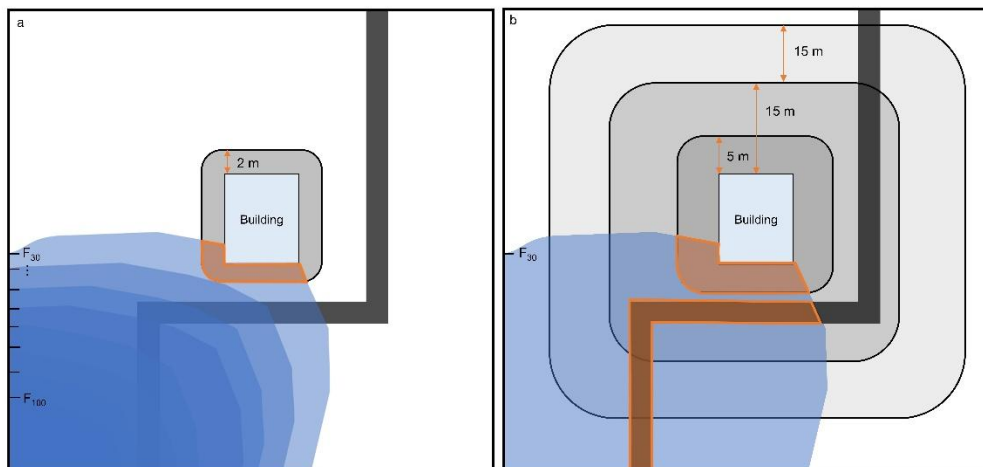
315 The assessment of the hazard to mobility and accessibility includes two tools. Using the first tool (see Figure S9 a and c), we determine the areas of intersection, expressed in square meters (labelled with A) and percentages (labelled with P), between the flood hazard layer and (a) a 5 m buffer around each building, representing the feasibility of accessing the building, and (b) 15 m and (c) 15-to-30 m buffers around affected buildings, capturing potential intersections with the road network.

320 The second tool (Fig. S9 b) includes the calculation of the actual hazard as described in von von Szombathely et al., (in review), where the hazard index related to mobility and accessibility (H_{MA}) is calculated using the maximum value derived from the Eq. 13.

$$H_{MA} = \text{Max}[F_X(4 \cdot A_{5m,30cm}), F_X(4 \cdot R_{15m,30cm}), F_X(4 \cdot R_{30m,30cm})] \quad (13)$$

There, $A_{5m,30cm}$ refers to the fraction of area within a 5 m buffer, which is flooded above a 30 cm water level. $R_{15m,30cm}$ and $R_{30m,30cm}$ describe the fraction of road area within a 15 m buffer and 15-to-30 m buffer, respectively, which are flooded 325 above a 30 cm water level.

To ensure relevant insights into surrounding road conditions and to exclude greater hazard ratings due to small flooded road areas, only flooded road areas exceeding 4 m² are included. A schematic drawing (Fig. 5) depicts the applied buffers and intersections applied. Figure S10 shows an excerpt of the resulting H_{MA} values.



330 **Figure 5: Schematic of the hazard concept.** (a) shows the schematic for the hazard of well-being, including flood levels (F) between 30 cm to 100 cm and a 2 m buffer around a building to assess water at the building as a threat to well-being (b) depicts the framework for the hazard of mobility and accessibility using a 5 m, 15 m and 15-30 m buffer around a building at a 30 cm flood level, taking into account high water levels on streets and blocked access to a building. Orange color highlights the flooded buffer around the building and the flooded road area.

335 3.2.4 Risk Tool

In a final calculation, the calculated sub-indices for social vulnerability, exposure and hazard are linked to obtain two specific risks during pluvial flooding events, one related to well-being (PFR_{WB}) and the other one related to mobility and accessibility (PFR_{MA}).



The PFR_{WB} is calculated as:

340 $PFR_{WB} = (SV_{PF})^a \cdot (E_{WB})^b \cdot (H_{WB})^c$ (14)

Where SV_{PF} reflects the social and economic characteristics that influence flood resilience, E_{WB} considers the number of ground-floor residents, as those are most vulnerable to direct flood impacts, and H_{WB} measures the likelihood and severity of floodwater intrusion at the ground floor level. Exponents a, b, and c reflects their corresponding (optional) weights.

$PFR_{MA} = (SV_{PF})^a \cdot (E_{MA})^b \cdot (H_{MA})^c$ (15)

345 With SV_{PF} reflecting the social and economic characteristics influencing flood resilience, E_{WB} considering the number of ground-floor residents, as those are most vulnerable to direct flood impacts, and H_{WB} measuring the likelihood and severity of floodwater intrusion at the ground floor level.

Within the toolbox, we provide further options by selecting the exponent for each sub-index (hazard, exposure and social vulnerability), which allows for further specific weighting of the sub-indices in the final risk assessment (see Figure S11).

350 An excerpt of the resulting risk values and related sub-indices is shown in the supplementary Figure S12. Additionally, we provide a tool to estimate the visualization classes (no risk to very high risk) based on an iterative mean-based filtering process. In this context, the absolute values themselves are not decisive, rather, the relative gradations between them determine the risk structure. This approach ensures that the classification of risk classes reflects the data's internal structure (see Fig. S13).

355 **4 Results and Discussion**

The resulting pluvial flood risk is provided by assessing the risk to well-being (Figure 6) and risk to mobility and accessibility (Figure 7).

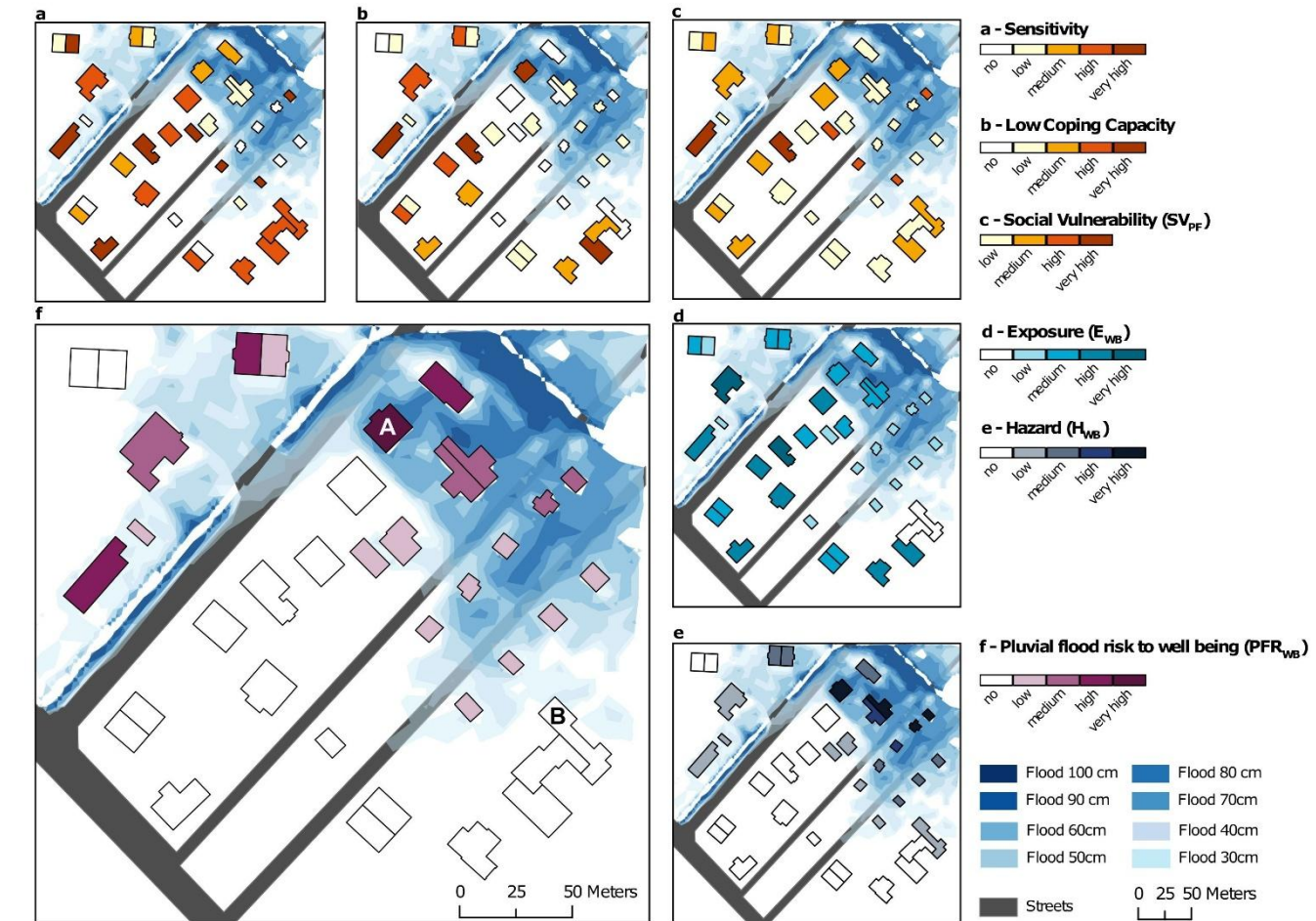
4.1. Risk to well-being

Using this example case study, we first present the pluvial flood risk to well-being as calculated by integrating social vulnerability, exposure and hazard. The composition of social vulnerability reveals how SV emerges from the interaction between sensitivity and coping capacity. Social vulnerability becomes high or very high for buildings with elevated sensitivity, for example due to the presence of young children or elderly residents living alone (indicated by darker red shades in Fig. 6 a). However, SV can be reduced where coping capacity is comparatively high (Fig. 6 b), resulting in an overall medium level of social vulnerability to pluvial flooding (Fig. 6 c). For the estimation of pluvial flood risk to well-being, exposure is limited to residents living on the ground floor, such as in mixed-use buildings with offices or stores on the ground level and apartments above. This highlights a potential limitation of this framework, where based on the building scale, case specific information is not captured, such as the building's entry side, the likelihood of water intrusion into the



basement, or the feasibility of implementing protective measures. However, the presented toolbox allows users to adjust the weighting of individual parameters, for instance by applying a higher weight to the sub-index to better reflect specific

370 conditions where necessary. Overall, the resulting risk map for well-being captures spatially differentiated patterns and helps



375 **Figure 6: Pluvial flood risk to well-being.** (a) shows sensitivity based on the presence of young children and elderly singles. (b) depicts the coping capacity and (c) the combination of both leading to the transformed social vulnerability index. (d) shows the exposure as the number of residents of the ground level per building, (e) depicts the hazard based on the 30 cm - 100 cm flood levels and (f) shows the final pluvial flood risk to well-being.



4.2. Risk to mobility and accessibility

380 Figure 7 presents the risk to mobility & accessibility with a focus on the street network under a flood depth of 30 cm. While social vulnerability remains identical to the assessment of risk to well-being (Fig. 7 a to c), the exposure is defined differently and now considers all residents per building (Figure 7 d). The corresponding hazard (Fig. 8 e) considers the flooded areas in close vicinity to the house (5 m) as well as flooded street segments located within distances of 15 m and 15 - 30 m.

385 The application of the pluvial flood risk toolbox revealed higher risks for buildings in close vicinity to flooded areas and streets, especially, where high exposure and high hazard categories coincide. This is exemplified by the building assigned to the highest risk class (see Building A in Figure 7 f). Notably, buildings with higher exposure, in this example due to larger building size (leading to possibly larger intersections with flooded areas) are assigned higher risk categories than smaller buildings with lower exposure, such as the single-family homes along the two streets (Example building B in Figure 7 f).

390 This is also due to the linear aggregation of exposure data from city sub-level to building scale.

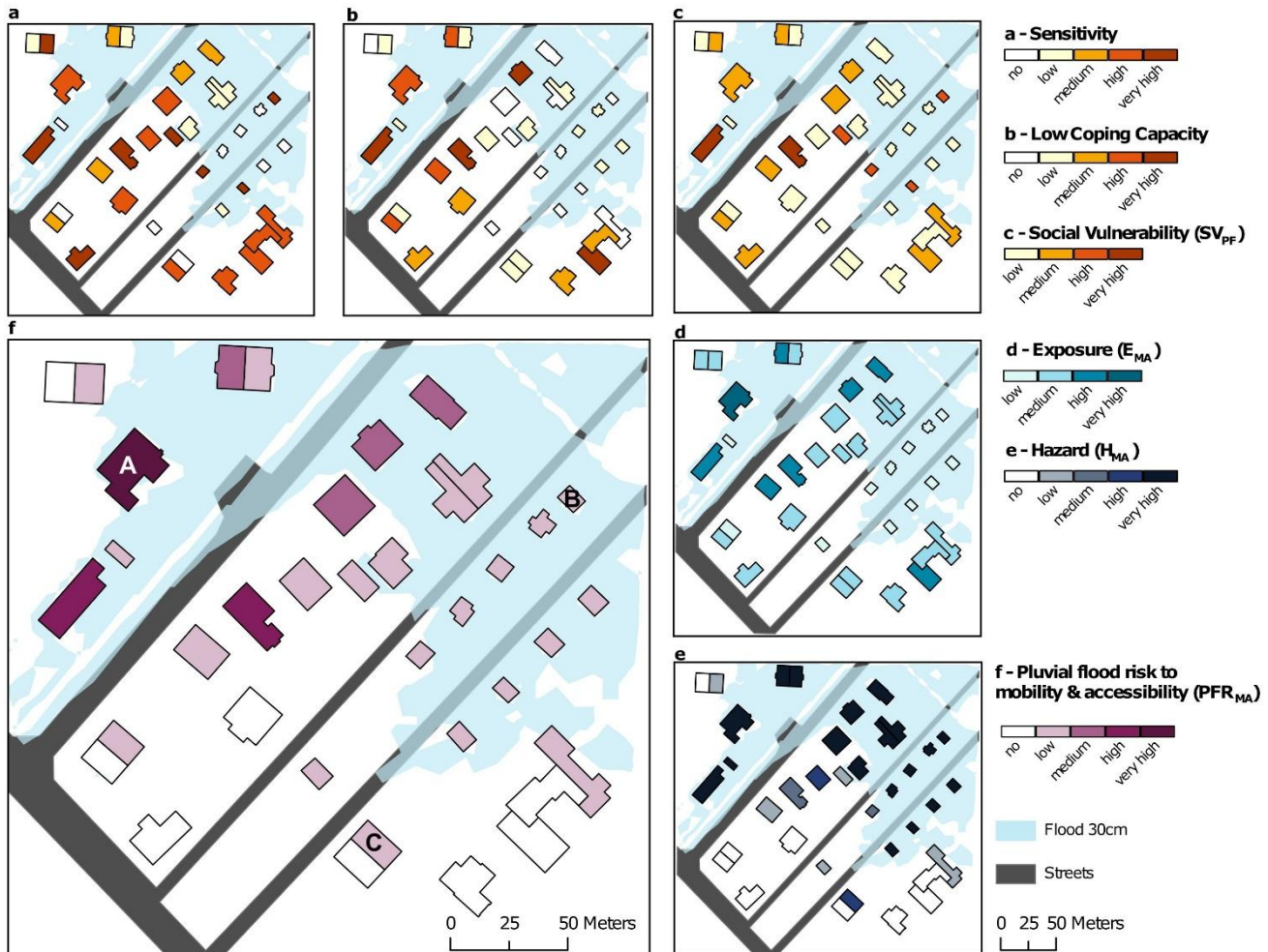
Some buildings (see e.g. Building B in Figure 7 f) were attributed a low risk to mobility and accessibility, even though for some houses the social vulnerability and hazard category were classified as high.

Besides the impact of the relatively low exposure, this captures a limitation of the framework when applied to a small example area with a high hazard level. It is related to the calculation of risk-classes, for which a mean-based classification

395 was applied to capture the distribution in the (example) area. Due to the high level of hazard in the study area, a relatively high share of houses is assigned with risk to mobility. If considering this framework for a whole city, the risk categories will be shifted, and the class of the example building B in this case would be assigned a higher risk class (see for example von Szombathely et al., (in review)). On the one hand, the relative risk assessment is a limitation, as the value itself cannot be interpreted (see also Russo et al. 2019). On the other hand, the relative nature of the framework allows to capture the

400 heterogeneity of the input data and provides a base for relative prioritization of necessary adaptation measures. Using this case example, we examine the behavior of the risk calculation on building level for typical urban building types, such as a city quarter in Hamburg. Semi-detached houses, consisting of two identical units sharing a common wall, show a distinct response within this framework. Within the toolbox we account for this by excluding the building area from the buffered area, resulting in a higher risk category to the side facing a flooded street, whereas the opposite side receives a lower or no

405 risk classification (see building C in Fig. 8 f). Although the calculation follows the risk framework, it reveals methodological shortcomings arising from the use of building-based data to infer risk for residents. For example, for two semi-detached houses with the same number of residents and same social vulnerability and hazard, the resulting risk index would increase, if the semi-detached buildings would be counted as one single building. In such cases, a careful interpretation by stakeholders and city management on a case-by-case basis is required.



410

Figure 7: Pluvial flood risk to mobility & accessibility. (a) shows sensitivity based on the presence of young children and elderly singles. (b) depicts the coping capacity and (c) the product of both leading to the transformed social vulnerability index. (d) shows the exposure as the number of residents per building, (e) depicts the hazard based on the 30 cm flood level and (f) shows the final pluvial flood risk to mobility & accessibility.

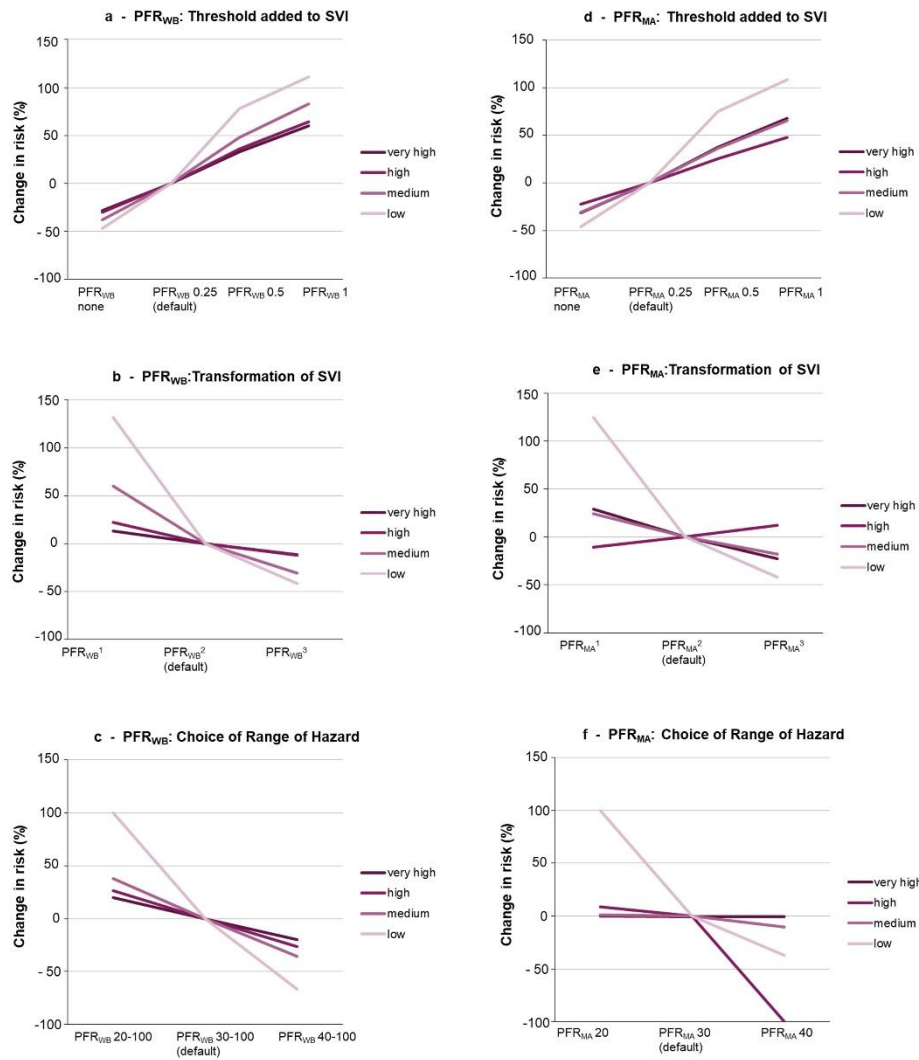
415

Nevertheless, this approach provides a viable framework for calculating high-resolution risk, effectively capturing both risks to well-being as well as to mobility and accessibility. The automated calculation implemented in the provided toolbox enables the transfer of this approach to real-world case studies and facilitates its application across different urban settings.



4.3 Sensitivity Analysis

420 The toolbox provides a framework for calculating explicit flood risk indicators but requires several context-dependent assumptions regarding parameter values and transformations. These choices can be flexibly adjusted, influencing the resulting risk indices. As the index classification is meaningful only in a relative sense, we assess its sensitivity by comparing changes in average relative risk across groups of buildings with similar risk characteristics.



425

Figure 8: Sensitivity analysis of the Pluvial Flood Risk (PFR) results. Panels (a,d) show the effect of adding a threshold to the SVI results; panels (b,e) show the effect of alternative SVI transformations; and panels (c,f) show the effect of varying the hazard range. Results are shown for four levels of the outcome variable (very high, high, medium, and low; corresponding to the figures in the results section). Default parameter settings are indicated on the x-axes.



430 **5 Limitations**

While this study provides a comprehensive framework for the assessment of pluvial flood risk in urban areas at the building level, several limitations must be accounted for:

- The estimation of risk including social vulnerability and exposure requires a high data resolution and current data. For the applied methodology, socio-economic data at the building resolution are required. Alternatively, data with coarser resolution can be disaggregated to the building level with the help of the toolsets provided in the pluvial flood risk toolbox. Disaggregation was applied for the analysis of pluvial flood risks in the city of Hamburg (von Szombathely et al. (in review)).
- The disaggregation to building-resolution requires several assumptions and case dependent adaptations which were highlighted in this study. By designing the toolbox to allow adjustments of hazard thresholds, the weighting of individual risk parameters, as well as the consideration of Shannon-Entropy, we aim to explicitly highlight those aspects where context-specific decisions are required.
- Pluvial floods may affect socially vulnerable groups disproportionately larger or smaller than indicated by the SVI. We mitigate this by using an additional transformation, the *flood sensitivity transformation*. For our case example based on data from Hamburg, we used the default values which were defined through a co-creation process with city authorities and informed by expert knowledge. However, we acknowledge that thresholds depend on local context and on the socio-economic data available and consequently they may have to be adapted to the individual study area.
- The representation of results on building scale may create an impression of false precision, as several important building-specific details cannot be adequately captured, such as the building's entry side, the likelihood of water intrusion into the basement, or the feasibility of implementing protective measures.
- The hazard indices do not consider flow velocities. In principle, water level or inundation depth are the main outputs of urban flood models, and therefore generally available for urban pluvial flood assessments (Guo et al., 2021). However, flow velocities might be relevant for mobility (Pregnolato et al., 2017) and damage to well-being (Jonkman & Penning-Rowsell, 2008).
- Although our risk implementation follows the IPCC risk framework, the model does not account for temporal changes or time dependent responses to the risk. The here used modelled hazard includes technical adaptation measures, such as sewer infrastructure and retention measures. This framework could extend to include further responses to risk and time domain by integrating agent-based modelling (Peng et al., 2023) or dynamic urban flood risk assessment (He et al., 2023). Including emergency response measures and long-term adaptation strategies would strengthen the model's applicability for decision-makers.



6 Conclusion and Outlook

We have outlined a possible approach for adapting the IPCC risk framework to urban environments and for estimating
465 pluvial flood risk at the building scale. Using a small synthetical case study based on empirical data from Hamburg, we demonstrated that shifting the spatial scale from sub-city units to individual buildings is generally feasible with the available data. However, working at this finer resolution requires several assumptions outlined in this study, such as differentiating risks based on exposure type, and applying generalizations where input data are not available at building scale, which is often the case given current data resolutions. To our knowledge, this represents the first publicly available application of the
470 IPCC framework at the building level in an urban context and showcases some challenges and opportunities with implementing this conceptual framework in a local context with empirical data. This finer level of granularity has the potential to significantly enhance the accuracy of urban risk assessments and support decision-making regarding disaster risk management and climate adaptation. The framework and toolbox, developed in close collaboration with city stakeholders through co-creation processes, enables such downscaling and provides a transferable structure that can be applied to other
475 cities as well. Due to its four-part structure, the toolbox can be adapted to other hazards, such as heat, though several adjustments of the risk parameters would be required and lies beyond the scope of this analysis.

While we do not claim that this is the optimal implementation, the framework offers a transparent method to quantify risk, determined by the risk for mobility and accessibility and risk to well-being. Our results underline the need for high-resolution and openly accessible data to meaningfully integrate hazard and exposure, a combination not extensively
480 documented in previous work. Given the increasing frequency and intensity of extreme events in the future (Sillmann et al., 2024) incorporating social vulnerability and hazard-dependent exposure into risk assessments is essential. The framework presented here offers municipal institutions a basis for identifying adaptation measures that go beyond a sole focus on the hazard and thus provide valuable guidance for urban flood risk management.

485



Supplement link

The link to the supplement will be included by Copernicus, if applicable.

Data availability

The toolbox presented in this outline, including the tools and input data needed to calculate the presented risk maps are
490 provided in Zenodo under: <https://doi.org/10.5281/zenodo.17986182>

Author contributions

Anastasia Vogelbacher: Writing – original draft, Methodology, Formal analysis, Data curation, Investigation, Visualization, Conceptualization. Malte von Szombathely: Writing – review & editing, Methodology, Formal analysis, Visualization, Conceptualization. Marc Lennartz: Writing – review & editing, Methodology, Data curation, Conceptualization. Benjamin
495 Poschlod: Writing – review & editing, Methodology, Conceptualization. Jana Sillmann: Writing – review & editing, Conceptualization, Resources.

Competing interests

The authors have no conflicts of interest to declare.

Acknowledgements

500 The authors thank the Deutsche Forschungsgemeinschaft (DFG, German Research Foundation) under Germany's Excellence Strategy–EXC 2037 'CLICCS- Climate, Climatic Change, and Society'– Project Number: 390683824. Resources provided by the Institute of Geo- Hydroinformatics at Hamburg University of Technology are greatly acknowledged.



References

505 Afifi, Z., Chu, H.-J., Kuo, Y.-L., Hsu, Y.-C., Wong, H.-K., Ali, M. Z., Afifi, Z., Chu, H.-J., Kuo, Y.-L., Hsu, Y.-C., Wong, H.-K., & Ali, M. Z. (2019). Residential Flood Loss Assessment and Risk Mapping from High-Resolution Simulation. *Water*, 11(4). <https://doi.org/10.3390/w11040751>

510 Alves, P. B. R., Djordjević, S., & Javadi, A. A. (2021). An integrated socio-environmental framework for mapping hazard-specific vulnerability and exposure in urban areas. *Urban Water Journal*, 18(7), 530–543. <https://doi.org/10.1080/1573062X.2021.1913505>

515 Arnbjerg-Nielsen, K., Willems, P., Olsson, J., Beecham, S., Pathirana, A., Bülow Gregersen, I., Madsen, H., & Nguyen, V.-T.-V. (2013). Impacts of climate change on rainfall extremes and urban drainage systems: A review. *Water Science and Technology*, 68(1), 16–28. <https://doi.org/10.2166/wst.2013.251>

520 Assumpção, T. H., Popescu, I., Jonoski, A., & Solomatine, D. P. (2018). Citizen observations contributing to flood modelling: Opportunities and challenges. *Hydrology and Earth System Sciences*, 22(2), 1473–1489. <https://doi.org/10.5194/hess-22-1473-2018>

Bertsch, R., Glenis, V., & Kilsby, C. (2022). Building level flood exposure analysis using a hydrodynamic model. *Environmental Modelling & Software*, 156, 105490. <https://doi.org/10.1016/j.envsoft.2022.105490>

525 Bhola, P. K., Leandro, J., & Disse, M. (2020). Building hazard maps with differentiated risk perception for flood impact assessment. *Natural Hazards and Earth System Sciences*, 20(10), 2647–2663. <https://doi.org/10.5194/nhess-20-2647-2020>

Bignami, D. F. (with Rosso, R., & Sanfilippo, U.). (2019). *Flood Proofing in Urban Areas*. Springer International Publishing AG.

Bourdieu, P. (1984). *Distinction: A social critique of the judgement of taste* (11. print). Harvard Univ. Press.

530 Bulti, D. T., & Abebe, B. G. (2020). A review of flood modeling methods for urban pluvial flood application. *Modeling Earth Systems and Environment*, 6(3), 1293–1302. <https://doi.org/10.1007/s40808-020-00803-z>

Calianno, M., Ruin, I., & Gourley, J. J. (2013). Supplementing flash flood reports with impact classifications. *Journal of Hydrology*, 477, 1–16. <https://doi.org/10.1016/j.jhydrol.2012.09.036>

535 Cea, L., & Costabile, P. (2022). Flood Risk in Urban Areas: Modelling, Management and Adaptation to Climate Change. A Review. *Hydrology*, 9(3), 50. <https://doi.org/10.3390/hydrology9030050>

Devi, K., Reddy, C. C., Rahul, K., Khuntia, J. R., & Das, B. S. (2025). A holistic methodology for evaluating flood vulnerability, generating flood risk map and conducting detailed flood inundation assessment. *Scientific Reports*, 15(1), 28253. <https://doi.org/10.1038/s41598-025-13025-z>

Dyson, B. (2017). Integration of Life Cycle Assessment Into Decision-Analytic Approaches for Sustainable Technologies. In *Encyclopedia of Sustainable Technologies* (pp. 81–89). Elsevier. <https://doi.org/10.1016/B978-0-12-409548-9.10037-5>

540 Ekmekcioğlu, Ö., Koc, K., & Özger, M. (2021). Stakeholder perceptions in flood risk assessment: A hybrid fuzzy AHP-TOPSIS approach for Istanbul, Turkey. *International Journal of Disaster Risk Reduction*, 60, 102327. <https://doi.org/10.1016/j.ijdrr.2021.102327>

Fereshtehpour, M., & Najafi, M. R. (2025). Urban stormwater resilience: Global insights and strategies for climate adaptation. *Urban Climate*, 59, 102290. <https://doi.org/10.1016/j.uclim.2025.102290>

FHH, Behörde für Stadtentwicklung und Wohnen. (2023). *Sozialmonitoring Integrierte Stadtteilentwicklung – Karten- und Tabellenband* 2023. FHH, BSW. <https://www.hamburg.de/resource/blob/286264/30117a83fe60f77cbd7344274fa5beb4/d-sozialmonitoring-bericht-2023-data.pdf>



FHH, Behörde für Stadtentwicklung und Wohnen. (2024). *Sozialmonitoring Integrierte Stadtteilentwicklung – Bericht 2024* (p. 31). FHH, BSW. <https://www.hamburg.de/resource/blob/1008718/43ed5565389b54c7af103ba038b658b0/d-sozialmonitoring-bericht-2024-data.pdf>

550 FHH, BUKEA. (2024). *Technisches Informationsblatt Starkregengefahrenkarte Hamburg* (p. 15). <https://www.hamburg.de/resource/blob/173730/5270f2cb96a1e41b5e45b64f84aa853e/d-technischesinformationsblatt-srgk-data.pdf>

555 FHH, Statistikamt Nord. (2017). *INSPIRE HH Verkehrsnetze ALKIS—MetaVer* (Geodatensatz, Vector Data No. <https://registry.gdi-de.org/id/de.hh/189b6adf-a805-42b7-a9ac-202da761fde2>; Version 3.2). MetaVer. <https://metaver.de/trefferanzeige?cmd=doShowDocument&docuuuid=1BD1BACC-6E6C-40E2-9B29-3B851CD6CFB5>

FHH, Statistikamt Nord. (2024, April 8). *Bevölkerung in Hamburg am 31.12.2023*. Statistisches Amt für Hamburg und Schleswig-Holstein. <https://www.statistik-nord.de/zahlen-fakten/hamburger-melderegister/bevoelkerungsstand#c6618>

560 Field, C. B., Barros, V. R., & Intergovernmental Panel on Climate Change (Eds.). (2014). *Climate change 2014: Impacts, adaptation, and vulnerability: Working Group II contribution to the fifth assessment report of the Intergovernmental Panel on Climate Change*. Cambridge University Press.

565 Fowler, H. J., Lenderink, G., Prein, A. F., Westra, S., Allan, R. P., Ban, N., Barbero, R., Berg, P., Blenkinsop, S., Do, H. X., Guerreiro, S., Haerter, J. O., Kendon, E. J., Lewis, E., Schaer, C., Sharma, A., Villarini, G., Wasko, C., & Zhang, X. (2021). Anthropogenic intensification of short-duration rainfall extremes. *Nature Reviews Earth & Environment*, 2(2), 107–122. <https://doi.org/10.1038/s43017-020-00128-6>

Fritsch, K., Assmann, A., & Tyrna, B. (2016). Long-term experiences with pluvial flood risk management. *E3S Web of Conferences*, 7, 04017. <https://doi.org/10.1051/e3sconf/20160704017>

570 Gentile, R., Cremen, G., Galasso, C., Jenkins, L. T., Manandhar, V., Menteşe, E. Y., Guragain, R., & McCloskey, J. (2022). Scoring, selecting, and developing physical impact models for multi-hazard risk assessment. *International Journal of Disaster Risk Reduction*, 82, 103365. <https://doi.org/10.1016/j.ijdrr.2022.103365>

He, H., Li, R., Pei, J., Bilodeau, J.-P., & Huang, G. (2023). Current overview of impact analysis and risk assessment of urban pluvial flood on road traffic. *Sustainable Cities and Society*, 99, 104993. <https://doi.org/10.1016/j.scs.2023.104993>

Hwang, C.-L., & Yoon, K. (1981). *Multiple Attribute Decision Making* (Vol. 186). Springer. <https://doi.org/10.1007/978-3-642-48318-9>

575 Intergovernmental Panel On Climate Change (Ipcc). (2021). *Climate Change 2021 – The Physical Science Basis: Working Group I Contribution to the Sixth Assessment Report of the Intergovernmental Panel on Climate Change* (1st ed.). Cambridge University Press. <https://doi.org/10.1017/9781009157896>

Jonkman, S. N., & Penning-Rowsell, E. (2008). Human Instability in Flood Flows¹. *JAWRA Journal of the American Water Resources Association*, 44(5), 1208–1218. <https://doi.org/10.1111/j.1752-1688.2008.00217.x>

580 Landesbetrieb Geoinformation und Vermessung (LGV) Hamburg. (2020). *INSPIRE HH Gebäude ALKIS—MetaVer* (Geodata, Vector data No. <https://registry.gdi-de.org/id/de.hh/e33c193f-278f-4118-a581-cc8e8420abc3>; Version 3.2). <https://metaver.de/trefferanzeige?docuuuid=0C4AD3A9-ECC4-4936-92FD-18E21DFA9234>

Lang, A., & Poschlod, B. (2024). Updating catastrophe models to today's climate – An application of a large ensemble approach to extreme rainfall. *Climate Risk Management*, 44, 100594. <https://doi.org/10.1016/j.crm.2024.100594>

585 Lazzarin, T., Viero, D. P., Molinari, D., Ballio, F., & Defina, A. (2022). Flood damage functions based on a single physics- and data-based impact parameter that jointly accounts for water depth and velocity. *Journal of Hydrology*, 607, 127485. <https://doi.org/10.1016/j.jhydrol.2022.127485>



Malekinezhad, H., Sepehri, M., Pham, Q. B., Hosseini, S. Z., Meshram, S. G., Vojtek, M., & Vojteková, J. (2021). Application of entropy weighting method for urban flood hazard mapping. *Acta Geophysica*, 69(3), 841–854.
590 https://doi.org/10.1007/s11600-021-00586-6

Nguyen, H. X., Nguyen, A. T., Ngo, A. T., Phan, V. T., Nguyen, T. D., Do, V. T., Dao, D. C., Dang, D. T., Nguyen, A. T., Nguyen, T. K., & Hens, L. (2020). A Hybrid Approach Using GIS-Based Fuzzy AHP–TOPSIS Assessing Flood Hazards along the South-Central Coast of Vietnam. *Applied Sciences*, 10(20), Article 20. https://doi.org/10.3390/app10207142

595 Nkwunonwo, U. C., Whitworth, M., & Baily, B. (2020). A review of the current status of flood modelling for urban flood risk management in the developing countries. *Scientific African*, 7, e00269. https://doi.org/10.1016/j.sciaf.2020.e00269

Pathan, A. I., Girish Agnihotri, P., Said, S., & Patel, D. (2022). AHP and TOPSIS based flood risk assessment- a case study of the Navsari City, Gujarat, India. *Environmental Monitoring and Assessment*, 194(7), 509. 600 https://doi.org/10.1007/s10661-022-10111-x

Peng, Y., Rodriguez Lopez, J. M., Santos, A. P., Mobeen, M., & Scheffran, J. (2023). Simulating exposure-related human mobility behavior at the neighborhood-level under COVID-19 in Porto Alegre, Brazil. *Cities*, 134, 104161. https://doi.org/10.1016/j.cities.2022.104161

605 Prall, M. C., Brandt, U. S., Halvorsen, N. S., Hansen, M. U., Dahlberg, N., & Andersen, K. J. (2024). A comprehensive approach for assessing social flood vulnerability and social flood risk: The case of Denmark. *International Journal of Disaster Risk Reduction*, 111, 104686. https://doi.org/10.1016/j.ijdrr.2024.104686

Rafiei-Sardooi, E., Azareh, A., Choubin, B., Mosavi, A. H., & Clague, J. J. (2021). Evaluating urban flood risk using hybrid method of TOPSIS and machine learning. *International Journal of Disaster Risk Reduction*, 66, 102614. https://doi.org/10.1016/j.ijdrr.2021.102614

610 Rehman, S., Sahana, M., Hong, H., Sajjad, H., & Ahmed, B. B. (2019). A systematic review on approaches and methods used for flood vulnerability assessment: Framework for future research. *Natural Hazards*, 96(2), 975–998. https://doi.org/10.1007/s11069-018-03567-z

Scalenghe, R., & Marsan, F. A. (2009). The anthropogenic sealing of soils in urban areas. *Landscape and Urban Planning*, 90(1–2), 1–10. https://doi.org/10.1016/j.landurbplan.2008.10.011

615 Shannon, C. E. (1948). A Mathematical Theory of Communication. *Bell System Technical Journal*, 27(3), 379–423. https://doi.org/10.1002/j.1538-7305.1948.tb01338.x

Sillmann, J., Raupach, T. H., Findell, K. L., Donat, M., Alves, L. M., Alexander, L., Borchert, L., De Amorim, P. B., Buontempo, C., Fischer, E. M., Franzke, C. L., Guan, B., Haasnoot, M., Hawkins, E., Jacob, D., Mahon, R., Maraun, D., Morrison, M. A., Poschlod, B., ... Županić, J. (2024). Climate extremes and risks: Links between 620 climate science and decision-making. *Frontiers in Climate*, 6, 1499765. https://doi.org/10.3389/fclim.2024.1499765

Statistisches Amt für Hamburg und Schleswig-Holstein. (2024). *Bevölkerung in Hamburg am 31.12.2023*. Statistisches Amt für Hamburg und Schleswig-Holstein. https://www.statistik-nord.de/fileadmin/Dokumente/Statistische_Berichte/bevoelkerung/A_I_S_1_j_H/A_I_S_1_j23.pdf

625 United Nations, Department of Economic and Social Affairs, Population Division (2019). *World Urbanization Prospects: The 2018 Revision* (ST/ESA/SER.A/420). New York: United Nations.

von Szombathely, M., Hanf, F. S., Bareis, J., Meier, L., Oßenbrügge, J., & Pohl, T. (2023). An Index-Based Approach to Assess Social Vulnerability for Hamburg, Germany. *International Journal of Disaster Risk Science*, 14(5), 782–794. https://doi.org/10.1007/s13753-023-00517-7

630 von Szombathely, Malte and Behrens, Jörn and Hanf, Franziska S. and Lennartz, Marc and Nayak, Shefali and Oßenbrügge, Jürgen and Poschlod, Benjamin and Scheffran, Juergen and Vogelbacher, Anastasia and Sillmann, Jana, Urban



Pluvial Flood Risk Mapping: A High-Resolution Assessment for the City of Hamburg. (*in review*) Available at SSRN: <https://ssrn.com/abstract=5231006> or <http://dx.doi.org/10.2139/ssrn.5231006>

Wilkinson, M. D., Dumontier, M., Aalbersberg, IJ. J., Appleton, G., Axton, M., Baak, A., Blomberg, N., Boiten, J.-W., da Silva Santos, L. B., Bourne, P. E., Bouwman, J., Brookes, A. J., Clark, T., Crosas, M., Dillo, I., Dumon, O., Edmunds, S., Evelo, C. T., Finkers, R., ... Mons, B. (2016). The FAIR Guiding Principles for scientific data management and stewardship. *Scientific Data*, 3(1), 160018. <https://doi.org/10.1038/sdata.2016.18>

635

Yang, W., Xu, K., Lian, J., Ma, C., & Bin, L. (2018). Integrated flood vulnerability assessment approach based on TOPSIS and Shannon entropy methods. *Ecological Indicators*, 89, 269–280. <https://doi.org/10.1016/j.ecolind.2018.02.015>